AMERICAN SOCIETY FOR MICROBIOLOGY | Journal of Virology

Herpes Simplex Virus 2 Virion Host Shutoff Endoribonuclease Activity Is Required To Disrupt Stress Granule Formation

Renée L. Finnen,[a] Mingzhao Zhu,[b]* Jing Li,[b] Daniel Romo,[c] Bruce W. Banfield[a]

Department of Biomedical and Molecular Sciences, Queen's University, Kingston, Ontario, Canada[a]; Department of Chemistry, Texas A&M University, College Station, Texas, USA[b]; Department of Chemistry and Biochemistry, Baylor University, Waco, Texas, USA[c]

ABSTRACT

We previously established that cells infected with herpes simplex virus 2 (HSV-2) are disrupted in their ability to form stress granules (SGs) in response to oxidative stress and that this disruption is mediated by virion host shutoff protein (vhs), a virion-associated endoribonuclease. Here, we test the requirement for vhs endoribonuclease activity in disruption of SG formation. We analyzed the ability of HSV-2 vhs carrying the point mutation D215N, which ablates its endoribonuclease activity, to disrupt SG formation in both transfected and infected cells. We present evidence that ablation of vhs endoribonuclease activity results in defects in vhs-mediated disruption of SG formation. Furthermore, we demonstrate that preformed SGs can be disassembled by HSV-2 infection in a manner that requires vhs endoribonuclease activity and that, befitting this ability to promote SG disassembly, vhs is able to localize to SGs. Together these data indicate that endoribonuclease activity must be maintained in order for vhs to disrupt SG formation. We propose a model whereby vhs-mediated destruction of SG mRNA promotes SG disassembly and may also prevent SG assembly.

IMPORTANCE

Stress granules (SGs) are transient cytoplasmic structures that form when a cell is exposed to stress. SGs are emerging as potential barriers to viral infection, necessitating a more thorough understanding of their basic biology. We identified virion host shutoff protein (vhs) as a herpes simplex virus 2 (HSV-2) protein capable of disrupting SG formation. As mRNA is a central component of SGs and the best-characterized activity of vhs is as an endoribonuclease specific for mRNA *in vivo*, we investigated the requirement for vhs endoribonuclease activity in disruption of SG formation. Our studies demonstrate that endoribonuclease activity is required for vhs to disrupt SG formation and, more specifically, that SG disassembly can be driven by vhs endoribonuclease activity. Notably, during the course of these studies we discovered that there is an ordered departure of SG components during their disassembly and, furthermore, that vhs itself has the capacity to localize to SGs.

Stress granules (SGs) are dynamic, non-membrane-bound cytoplasmic compartments that contain translationally silent mRNAs that remain associated with a cadre of translation initiation proteins, poly(A) binding protein (PABP), and the small ribosomal subunit in the form of messenger ribonucleoprotein complexes (mRNPs) (1). SGs assemble rapidly in response to a variety of stressful conditions and likewise can disassemble rapidly when stress is alleviated. Natural stresses that eukaryotic cells encounter include starvation, elevated temperature (heat shock), oxidation, and virus infection, all of which can be sensed by four distinct eukaryotic initiation factor 2 (eIF2) kinases. Following the sensing of stress, these kinases become activated and phosphorylate the alpha subunit of eIF2 (eIF2α), leading to a failure to initiate new rounds of translation (2). The ensuing stoppage in protein synthesis causes a sudden increase in mRNPs that are no longer associated with translating ribosomes. An increase in cytoplasmic levels of free mRNPs has been proposed to be the seminal event that initiates the assembly of SGs (1, 3). This notion is supported by observations that compounds that stop protein synthesis by means that are mechanistically distinct from eIF2α phosphorylation, such as puromycin and pateamine A (PatA), promote SG formation (4–6), while compounds that keep mRNAs associated with 80S ribosomes, such as cycloheximide and emetine, discourage SG formation (6). Further experimental verification of the governing role of cytoplasmic levels of mRNPs in SG assembly was recently provided by Pastré and colleagues, who demonstrated that delivery of exogenous single-stranded nucleic acid (RNA or DNA) to cells could promote SG formation (7), and by the recent *in vitro* studies of Cech and colleagues, who demonstrated that the formation of higher-order assemblages of the RNA binding protein FUS (*fu*sed in *s*arcoma) could be seeded by the addition of RNA (8). The steps leading from an increase in cytoplasmic levels of free mRNPs to assembly of microscopically visible cytoplasmic granules with a complex protein composition are ill defined. The contribution of cellular proteins with both RNA binding capacity and prion-like domains, such as Ras-GTPase-activating SH3-domain-binding protein (G3BP) (9) and T cell internal antigen 1 (TIA-1) (10), as well as many posttranslational modifications, including dephosphorylation (9), methylation (11, 12), deacetylation (13), ubiquitination (13), *O*-GlcNac

Received 13 May 2016 **Accepted** 20 June 2016

Accepted manuscript posted online 22 June 2016

Citation Finnen RL, Zhu M, Li J, Romo D, Banfield BW. 2016. Herpes simplex virus 2 virion host shutoff endoribonuclease activity is required to disrupt stress granule formation. J Virol 90:7943–7955. doi:10.1128/JVI.00947-16.

Editor: R. M. Sandri-Goldin, University of California, Irvine

Address correspondence to Bruce W. Banfield, bruce.banfield@queensu.ca.

* Present address: Mingzhao Zhu, Department of Chemistry and Biochemistry, Baylor University, Waco, Texas, USA.

modification (14), and poly(ADP ribosyl)ation (PARylation) (15–17), have all been implicated in the assembly of these cytoplasmic compartments. Weak intermolecular interactions facilitated by RNA binding proteins with prion-like domains in combination with these various posttranslational modifications have been proposed to allow mammalian SGs to exist in a liquid droplet-like state (18). Interactions between mRNPs and the cytoskeleton also contribute to SG assembly (19–23). The conventional model of SG assembly along with the physical state in which SGs exist has been challenged by recent work published by Parker and colleagues. Their analysis of SGs using superresolution microscopy suggests that SGs have a stable core structure surrounded by a more dynamic shell (24). Like SG assembly, SG disassembly can also occur rapidly and is mechanistically ill defined. Reversal of some of the posttranslational modifications implicated in SG assembly can cause SG disassembly. For example, phosphorylation of SG proteins G3BP and dual-specificity tyrosine-phosphorylation-regulated kinase 3 (DYRK3) leads to disassembly of SGs (9, 25), as does removal of poly(ADP ribose) (PAR) modifications by PAR glycohydrolases (16).

We have established that cells infected with herpes simplex virus 2 (HSV-2) have a disruption in their ability to form SGs in response to treatment with arsenite, an inducer of oxidative stress (26). The ability to form SGs in response to arsenite was restored in cells infected with HSV-2 strains carrying a defective virion host shutoff protein (vhs), implicating vhs as a viral protein involved in disrupting arsenite-induced SG formation (27). Furthermore, disruption of arsenite-induced SG formation can be observed in cells transfected with a vhs expression plasmid, indicating that vhs can mediate this disruption in the absence of other viral proteins (27). vhs is a endoribonuclease (28, 29) encoded by the UL41 gene (30, 31) and is a component of the tegument layer of alphaherpesvirus virions (32, 33). Packaging of vhs into virions allows this endoribonuclease to be delivered to the cytoplasm immediately upon fusion of viral and cellular membranes and to commence the degradation of cellular mRNAs in advance of *de novo* viral gene expression. Cleavage of most mRNAs by vhs *in vivo* occurs within the 5′ untranslated region near the cap, and the resulting decapped mRNAs are then rapidly degraded by the cellular 5′→3′ exonuclease XrnI (34, 35). Degradation of cellular mRNAs in combination with disruptions in cellular mRNA biogenesis mediated by the immediate early viral protein ICP27 led to considerable suppression of cellular protein synthesis (36, 37). Targeting of vhs activity toward mRNAs *in vivo* may be facilitated by its ability to bind the cellular translation initiation factors eIF4A, eIF4B, and eIF4H (38–40). The ability of vhs to bind to translation initiation factors may also be indicative of a direct role for vhs in translation. Cap-independent translation via *cis*-acting elements and enhanced translation of viral late mRNAs have both been ascribed to vhs (41–44). As vhs may interact with mRNA in two distinct manners and has the ability to bind eIF4A, eIF4B, and eIF4H, all of which are known SG components (45), predicting how vhs is able to disrupt arsenite-induced SG formation is not straightforward.

The primary objective of this study was to examine the impact of vhs endoribonuclease activity on SG formation. vhs shares sequence homology with the flap endonuclease 1 (FEN-1) family of endonucleases (28), and the amino acids essential for the endoribonuclease activity of HSV-1 vhs have been thoroughly mapped (40, 46). These mapping studies demonstrated that changing aspartic acid 213 of HSV-1 vhs to asparagine (D213N) resulted in a protein that lacked endoribonuclease activity yet retained the ability to bind both eIF4A and eIF4H. The analogous aspartic acid in human FEN-1, aspartic acid 179, helps coordinate a metal ion-binding pocket in the active site that is critical for catalytic activity (47, 48). HSV-2 vhs shares 86% amino acid identity with HSV-1 vhs (49), and the analogous mutation in HSV-2 vhs (D215N) also selectively ablates endoribonuclease activity (50). Utilizing a D215N version of HSV-2 vhs, we present evidence that ablation of vhs endoribonuclease activity results in defects in vhs-mediated disruption of SG formation. We also demonstrate that preformed SGs can be disassembled by HSV-2 infection in a manner that requires the endoribonuclease activity of vhs and that, befitting this ability to promote SG disassembly, vhs is able to localize to SGs. We propose a model whereby destruction of mRNA by vhs promotes SG disassembly and/or prevents SG assembly. This model is in keeping with the seminal role proposed for RNA in initiating SG formation and furthermore predicts that intact RNA is crucial for maintaining the integrity of these cytoplasmic compartments.

MATERIALS AND METHODS

Cells and viruses. African green monkey kidney cells (Vero), cervical carcinoma cells (HeLa), and A549 cells that stably produce enhanced green fluorescent protein (EGFP)-G3BP1 (A549 SGG) (51) were maintained in Dulbecco's modified Eagle's medium (DMEM) supplemented with 10% fetal bovine serum (FBS) in a 5% CO_2 environment. HSV-2 strain 186 virus (wild type [WT]) and ΔUL41 virus (27) as well as the D215N and repaired D215N (D215NRep) derivative viruses generated for this study, were all propagated on Vero cells, and their titers were determined on Vero cells. To generate a high-titer stock of D215N virus to facilitate high-multiplicity of infection (MOI) infections, confluent 150-mm dishes of Vero cells were inoculated at an MOI of 0.01 and then incubated for 2 to 3 days at 34°C. Infected cells and medium were harvested together, and then infected cells were separated from medium by centrifugation at 1,100 × *g* for 5 min. The infected cell fraction was resuspended in SPGA buffer (218 mM sucrose, 3.8 mM KH_2PO_4, 7.2 mM K_2HPO_4, 4.9 mM sodium glutamate, 1% [wt/vol] bovine serum albumin [BSA], 10% FBS), and then cells were lysed by vortexing with sterile glass beads (425 to 600 μm [Sigma, St. Louis, MO]). The infected cell lysate was centrifuged at 2,000 × *g* for 5 min, and the resulting supernatant was aliquoted and stored at −80°C. Stocks of WT, D215NRep, and ΔUL41 virus were prepared and stored in a similar manner. Unless otherwise indicated, infection times refer to the length of time following a 1-h inoculation period.

Construction of recombinant HSV-2 strains. pYEbac373, the full-length infectious HSV-2 186 bacterial artificial chromosome (BAC), was constructed as described previously (52). A BAC carrying full-length vhs with the point mutation D215N was constructed by the two-step Red-mediated recombination procedure, using pYEbac373 in *Escherichia coli* GS1783 (53).

Forward primer 5′-TCCAGGCCCAGTTTCGCCTTTTCC-3′ and reverse primer 5′-GGTCAGCGTAGGCATGCTCTCCAG-3′ were used to amplify a product from pRF97 (described below) for the initial recombination step. Restriction fragment length polymorphism analysis following EcoRI digestion was used to confirm the overall integrity of each recombinant BAC clone. Additionally, PCR fragments amplified from each recombinant BAC clone and from DNA isolated from the reconstituted D215N virus were sequenced to verify that recombination had occurred at the correct location within the viral genome, to verify that the D215N mutation was present, and to verify that no additional mutations were present within UL41. Virus was reconstituted from BAC DNA by transfection of Vero cells as described previously (52). A similar strategy was used to repair the D215N mutation (D215NRep) using a product amplified from pRF87 (27) for the initial recombination step.

Single-step replication analysis. A total of 5×10^5 Vero cells were seeded into 6-well dishes 1 day prior to infection. Vero cell monolayers (approximately 1×10^6 cells per well) were infected at an MOI of 3. All infections were performed in duplicate. After a 1-h inoculation period, monolayers were treated for 2 min at 37°C with low-pH citrate buffer (40 mM Na citrate, 10 mM KCl, 135 mM NaCl [pH 3.0]) to inactivate extracellular virions, washed once with medium, and then incubated at 37°C. Infected monolayers were collected by scraping cells and medium together at 0, 4, 8, 12, 24, and 48 h postinoculation and stored at −80°C. Samples were frozen at −80°C and thawed at 37°C twice and sonicated, and the cellular debris was removed from the cell lysate by centrifugation. The virus titers of the clarified lysates were determined in duplicate by plaque assay on Vero cells.

Plasmids and transfections. The construction of an expression plasmid containing wild-type (WT) UL41, pRF78, was described previously (27). A D215N mutation was introduced into the WT UL41 gene contained within pRF78 by mutagenic PCR using forward primer 5′-GTAC GTGCATACCACGAATACCGATCTCCTGC-3′ and reverse primer 5′-GCAGGAGATCGGTATTCGTGGTATGCACGTAC-3′. The resulting plasmid, pRF96, was sequenced to ensure that no spurious mutations were introduced into UL41 during construction. To construct a D215N UL41 expression plasmid containing an I-SceI-flanked kanamycin cassette with repeated UL41-derived sequence for facilitating two-step Red-mediated recombination, an AscI fragment derived from pRF87, described previously (27), was ligated to AscI-digested pRF96. The resulting plasmid, pRF97, was screened for the ability to confer kanamycin resistance and for correct orientation of the approximately 1,100-bp AscI fragment by NotI digestion. An expression plasmid encoding an internally gutted (IG) version of UL41 missing codons 24 through 474 was constructed by digesting pRF78 with ApaI then religating the digested plasmid. The resulting plasmid, pRF93, was then screened for loss of the approximately 1,300-bp ApaI fragment. A myc tag was introduced on to the amino terminus of D215N UL41 by annealing forward primer 5′-CTAGCATGGAGCAGAAACTCATCTCTGAAGAGGATCTGGG-3′ to reverse primer 5′-AATTCCCAGATCCTCTTCAGAGATGAGTTTCTG CTCCATG-3′ to form a cassette containing myc tag coding sequence flanked with NheI- and EcoRI-compatible cohesive ends. This cassette was ligated into NheI/EcoRI-cut pRF96, and the resulting plasmid, pRF99, was screened for loss of XhoI from the multiple-cloning site and sequenced to ensure that the myc tag coding sequence was in frame with D215N UL41. The mCherry red fluorescent protein expression plasmid, pJR70, is a pEGFP-N1-based expression vector in which the enhanced green fluorescent protein (EGFP) gene was replaced with the mCherry gene (B. W. Banfield and J. A. Randall, unpublished data). *Renilla* luciferase expression plasmid pRLSV40 was acquired from Promega (Promega, Madison, WI). Transfection of HeLa cells was carried out using X-treme GENE HP DNA transfection reagent (Roche, Laval, QC, Canada) according to the manufacturer's protocols.

Induction of SGs. To induce SG formation, HeLa cells were treated with 0.5 mM arsenite (Sigma, St. Louis, MO) for 30 min or 300 nM desmethyl desamino pateamine A (DMDA PatA) (54) for 30 min at 37°C.

Immunological reagents. Goat polyclonal antiserum against human TIA-1 (Santa Cruz Biotechnology, Santa Cruz, CA) was used for indirect immunofluorescence microscopy at a dilution of 1:500. Mouse monoclonal antibody against human G3BP (BD Biosciences, Mississauga, ON, Canada) was used for indirect immunofluorescence microscopy at a dilution of 1:1,000. Mouse monoclonal antibody against HSV ICP27 (Virusys, Taneytown, MD) was used for indirect immunofluorescence microscopy at a dilution of 1:1,000. Rat polyclonal antiserum against HSV-2 Us3 (55) was used for indirect immunofluorescence microscopy at a dilution of 1:500. Mouse monoclonal antibody against the myc tag (Roche, Laval, QC, Canada) was used for immunofluorescence microscopy at a dilution of 1:200. Rabbit polyclonal antiserum against HSV vhs (56) was used for Western blotting at a dilution of 1:3,000. Mouse monoclonal antibody against HSV ICP5 (Virusys, Taneytown, MD) was used for Western blotting at a dilution of 1:500. Alexa Fluor 488-conjugated donkey anti-goat IgG, Alexa Fluor 488-conjugated donkey anti-mouse IgG, Alexa Fluor 488-conjugated donkey anti-rat IgG, Alexa Fluor 568-conjugated donkey anti-mouse IgG, Alexa Fluor 647-conjugated donkey anti-mouse IgG, and Alexa Fluor 647-conjugated chicken anti-rat IgG (Molecular Probes, Eugene, OR) were all used for indirect immunofluorescence at a dilution of 1:500. Horseradish peroxidase-conjugated goat anti-mouse IgG and horseradish peroxidase-conjugated goat anti-rabbit IgG (Sigma, St. Louis, MO) were used for Western blotting at a dilution of 1:10,000.

Indirect immunofluorescence microscopy. Cells for microscopic analyses were grown on either glass coverslips or glass bottom dishes (MatTek, Ashland, MA). Cells were fixed and stained as described previously (55). Stained cells were examined using either a Nikon Eclipse TE200 inverted fluorescence microscope and Metamorph 7.1.2.0 software or an Olympus FV1000 laser scanning confocal microscope and Fluoview 1.7.3.0 software. Images from the confocal microscope were captured using a 60× (1.42-numerical aperture [NA]) oil immersion objective. Composites of representative images were prepared using Adobe Photoshop software. Unpaired *t* tests of data yielded from microscopic analyses were performed using GraphPad QuickCalcs.

Analysis of vhs packaging. For analysis of vhs packaging, virions were purified as described previously (57). Confluent 150-mm dishes of Vero cells were inoculated for 1 h at an MOI of 0.01. Two to 3 days later, medium was collected. Collected medium was centrifuged three times in succession at $1{,}100 \times g$ to pellet detached cells and cellular debris. The clarified supernatant was layered over a cushion of 30% (wt/vol) sucrose in phosphate-buffered saline (PBS) and centrifuged in a Beckman SW28 rotor at 23,000 rpm for 3 h. Pelleted virions were resuspended in 50 μl of 1× SDS-PAGE loading buffer. Solubilized virions were then boiled for 5 min and stored at −20°C prior to Western analyses. Western analyses of virion preparations were performed as described previously (27).

RESULTS

vhs endonuclease activity is required to disrupt SG formation in transfected cells. We developed a transfection-based assay to examine vhs endoribonuclease activity alongside vhs SG disruption activity (Fig. 1A). HeLa cells were transfected with a mixture containing equivalent amounts of vhs expression plasmid, an mCherry expression plasmid for detection of transfected cells by microscopy, and plasmid pRLSV40 for indirect monitoring of endoribonuclease activity by assaying *Renilla* luciferase activity. In these assays, we compared cells transfected with the wild-type (WT) vhs expression plasmid to cells transfected with the endoribonuclease-deficient vhs expression plasmid carrying a D215N mutation in vhs and utilized an internally gutted (IG) vhs expression plasmid as a normalization control. IG vhs was constructed by deleting the sequence contained between two internal in-frame ApaI sites in the WT UL41 gene (Fig. 1B). This deletion removes most of the coding capacity of UL41 (codons 24 through 474) while maintaining the capacity for translation initiation and termination on mRNA transcripts generated from this construct. The IG vhs expression plasmid performed similarly to the pCI-neo parent vector in pilot luciferase assays (data not shown) and IG vhs was used as a normalization control in subsequent luciferase assays. Cells transfected with WT vhs expression plasmid had considerably reduced luciferase activity in comparison to cells transfected with IG vhs (Fig. 1C). In contrast, levels of luciferase activity were not significantly different between IG and D215N transfections ($P = 0.2784$), consistent with lack of endonuclease activity in HSV-2 D215N vhs.

For our initial SG disruption assays, we treated transfected cells with 0.5 mM arsenite to induce SG formation and then measured the percentage of cells with visible SGs following staining for the

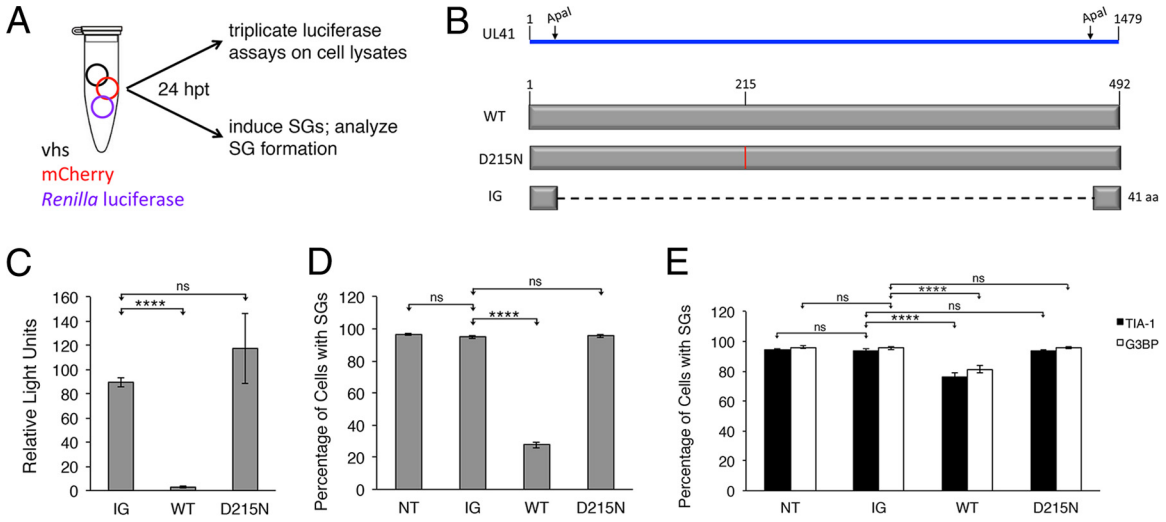

FIG 1 Transfection-based assay to examine HSV-2 endonuclease activity and SG disruption. (A) HeLa cells transfected with equivalent amounts of HSV-2 vhs, mCherry, and luciferase expression constructs were analyzed at 24 h posttransfection (hpt). (B) HSV-2 vhs expression constructs examined. The HSV-2 UL41 gene that encodes vhs is depicted by the blue line; vhs proteins are depicted by the gray bars. The red line indicates point mutation D215N, which was introduced into full-length wild-type (WT) vhs to ablate its endoribonuclease activity. An internally gutted (IG) version of vhs was used as a normalization control. The dashed line in IG vhs indicates an internal deletion of codons 24 to 474, generated by excising an in-frame ApaI fragment from UL41. (C) Results of luciferase assays. Twenty microliters of lysates prepared from triplicate transfections or from nontransfected (NT) background controls was assayed using Promega's Stop&Glo reagent. Raw values were adjusted for background, and then the highest value obtained in the adjusted normalization control (IG) was set to 100, and other values were scored relative to it. Data for the IG vhs were compiled from four independent experiments performed in triplicate; data for the WT and D215N versions were compiled from three independent experiments performed in triplicate. Error bars indicate standard errors of the means. Unpaired *t* tests on adjusted, normalized data were performed using GraphPad QuickCalcs. ****, $P < 0.0001$; ns, difference not statistically significant. (D and E) SG disruption results. Transfected cells were treated with 0.5 mM arsenite (D) or 300 nM DMDA PatA (E) for 30 min and then fixed. Samples in panel D were stained with goat polyclonal antiserum specific for TIA-1 followed by staining with Alexa Fluor 488-conjugated donkey anti-goat IgG. Samples in panel E were stained with goat polyclonal antiserum specific for TIA-1 followed by staining with Alexa Fluor 488-conjugated donkey anti-goat IgG or with mouse monoclonal antibody specific for G3BP followed by staining with Alexa Fluor 488-conjugated donkey anti-mouse IgG. Samples were examined on an inverted epifluorescence microscope, and the percentage of cells with SGs was scored in 10 fields per sample. Data in panel D were compiled from two independent experiments. Data in panel E were generated by scoring duplicate transfections stained for either TIA-1 or G3BP and were compiled from two independent experiments. Transfection efficiency was estimated by scoring the percentage of cells expressing mCherry in 10 fields of IG transfections. Error bars indicate standard errors of the means. ****, $P < 0.0001$; ns, difference not statistically significant.

SG marker TIA-1. Arsenite treatment promotes the phosphorylation of eIF2α in a heme-regulated inhibitor kinase-dependent manner leading to translational arrest and the subsequent formation of SGs (58). Cells transfected with IG vhs performed comparably to nontransfected (NT) cells following arsenite treatment (Fig. 1D), indicating that transfection alone did not disrupt arsenite-induced SG formation. SG disruption was readily detected in cells transfected with WT vhs, and the fraction of cells lacking SGs (approximately 65%) roughly corresponded to the transfection efficiency in these experiments, predicted from averaged transfection efficiencies observed in IG transfections to be 58%. SG disruption was not observed in cells transfected with D215N vhs. These data demonstrate that vhs endoribonuclease activity is required to disrupt arsenite-induced SG formation in transfected cells.

SG formation can also be induced by means that are independent of eIF2α phosphorylation. Pateamine A (PatA), a natural product isolated from sea sponge, and its synthetic derivative desmethyl desamino (DMDA) PatA are potent modulators of eIF4A that also cause translational arrest and SG formation (4, 5, 54, 59–61). In our initial studies on the impact of HSV-2 infection on SG formation, we found that infection interfered with the formation of arsenite-induced SGs but did not interfere with the formation of PatA-induced SGs (26). However, the SGs that formed in HSV-2-infected cells following PatA treatment were largely devoid of the SG marker TIA-1. To determine if these differential effects on SG formation would also be seen in vhs-transfected cells, we treated transfected cells with 300 nM DMDA PatA to induce SGs and then measured the percentage of cells with visible SGs. In order to detect differences in SG composition, this experiment was performed in duplicate, samples were stained for either TIA-1 or G3BP, and measurements of the percentage of cells with visible SGs was performed using each marker independently (Fig. 1E). Disruption of DMDA PatA-induced SGs was observed in cells transfected with WT vhs but not in cells transfected with D215N vhs. Similar levels of SG disruption were seen in WT transfections regardless of which SG marker was followed for quantitation, and the fraction of cells lacking SGs (approximately 24% for TIA-1 and 19% for G3BP; $P = 0.1697$) again roughly corresponded to the transfection efficiency in these experiments, predicted from averaged transfection efficiencies observed in IG transfections (approximately 29% for TIA-1 and 28% for G3BP). Thus, when overexpressed, vhs can disrupt SG formation caused by either eIF2α phosphorylation-dependent or eIF2α phosphorylation-independent mechanisms of translational arrest, and vhs-mediated disruption of SG formation requires endoribonuclease activity.

Disruption of SG formation by HSV-2 carrying an endonuclease-deficient vhs. To examine the requirement for vhs endoribonuclease activity in SG disruption in infected cells, we utilized *en passant* mutagenesis to construct an HSV-2 strain 186 virus

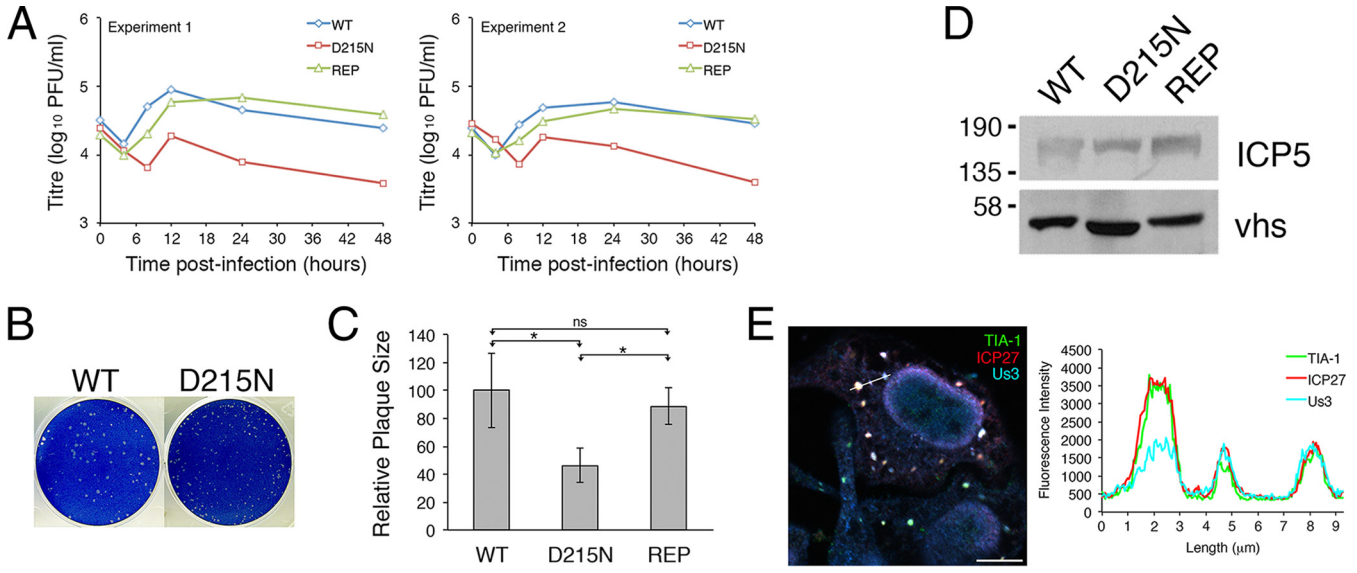

FIG 2 Characterization of D215N virus. (A) Vero cells were inoculated in duplicate at an MOI of 3 for 1 h, extracellular virus was inactivated by treatment with low-pH citrate buffer, medium was replaced, and infected cells and medium were harvested together at the indicated time points. Harvested infected cells were frozen and thawed twice and then centrifuged, and the clarified supernatants were titrated in duplicate on Vero cells. Each data point is the average of duplicate values. The results from two independent experiments are shown. (B) Viral plaques were allowed to form on Vero cells for 3 days and then fixed and stained with 70% methanol containing 0.5% methylene blue. (C) Viral plaques were allowed to form on Vero cells for 24 h and then fixed and stained with rat polyclonal antiserum specific for Us3 followed by staining with Alexa Fluor 488-conjugated donkey anti-rat IgG. For each virus, images of 40 plaques were captured on an inverted epifluorescence microscope using a 4× objective. The area of plaques from these images was measured using Image-Pro Plus version 6.3 software. The largest plaque area measured for the WT was set to 100, and other values were scored relative to it. Error bars indicate standard errors of the means. *, $P < 0.1$; ns, difference not statistically significant. (D) Virion preparations were separated on an SDS–8% polyacrylamide gel and transferred to a polyvinylidene difluoride (PVDF) membrane. The membrane was blocked overnight at 4°C in Tris-buffered saline with Tween 20 (TBST) containing 3% bovine serum albumin (BSA), and the blocked membrane was probed for the presence of major capsid protein (ICP5) or vhs. Positions of molecular mass markers in kilodaltons are indicated on the left. (E) HeLa cells were infected with D215N virus at an MOI of 4. At 5 hpi, infected cells were fixed and stained with goat polyclonal antiserum specific for TIA-1, mouse monoclonal antibody specific for ICP27, and rat polyclonal antiserum specific for Us3 followed by staining with Alexa Fluor 488-conjugated donkey anti-goat IgG, Alexa Fluor 568-conjugated donkey anti-mouse IgG, and Alexa Fluor 647-conjugated chicken anti-rat IgG. Stained cells were examined by confocal microscopy, and a representative merged image of an infected cell containing spontaneous SGs is shown. The scale bar is 10 μm. The fluorescence intensity was measured across an approximately 9-μm line drawn between adjacent SGs using Fluoview 1.7.3.0 software. The location of the measurement line is shown on the merged image.

carrying a D215N mutation in vhs and to subsequently repair this mutation (D215NRep). D215N virus exhibited a growth deficiency in comparison to WT and D215NRep viruses on Vero cells (Fig. 2A) and formed smaller plaques than either WT or D215NRep on Vero cells (Fig. 2B and C). Importantly, no defects in vhs packaging were observed with D215N vhs (Fig. 2D), meaning that similar levels of WT or D215N vhs would be delivered to cells upon entry. The vhs produced in cells infected with D215N virus showed a slight increase in electrophoretic mobility compared to the vhs produced in cells infected with WT or D215NRep viruses (Fig. 2D). A similar observation was made with HSV-2 strain 333 carrying a D215N vhs (50). We previously reported that cells infected with HSV-2 viruses carrying either a deletion of most of the UL41 coding sequence (ΔUL41) or a frameshift mutation in UL41 at codon 343 formed spontaneous SGs late in infection (27). Spontaneous SGs were observed in approximately 12% (39 of 319) of HeLa cells infected with D215N virus at an MOI of 4 at 5 h postinfection (hpi). In keeping with our previous observations (27), these SGs contained both ICP27 and Us3 (Fig. 2E).

To compare disruption of SG formation in infected cells, HeLa cells were infected with WT, D215N, or D215NRep viruses at an MOI of 4 or mock infected and then treated with either 500 mM arsenite or 300 nM DMDA PatA at 4 hpi to induce SGs or left untreated (data not shown). Infected cells were then fixed and stained for the presence of TIA-1 and G3BP. Infectivity controls on virus-infected samples confirmed that all cells were infected under these conditions (data not shown). As shown in the top half of Fig. 3A, cells infected with WT or D215NRep virus displayed a disruption in their ability to form SGs in response to arsenite treatment as indicated by a drastic decrease in the fraction of cells with SGs (both less than 1% compared to greater than 98% in mock-infected cells treated with arsenite). Cells infected with D215N virus also showed a large decrease in the fraction of cells with SGs (8%). This value was greater than that observed in untreated cells infected with D215N (less than 1%), indicating that, at this time postinfection, spontaneous SG formation was not contributing significantly to this value. A large decrease in the fraction of cells with SGs was also observed when cells were infected at a high MOI with ΔUL41 virus (Fig. 3B), and this decrease was comparable to that of D215N virus in this experiment. These data suggest that an additional viral component or components may be involved in disrupting arsenite-induced SG formation. This possibility may have gone undetected in our previous characterization of disruption of arsenite-induced SG formation by ΔUL41 virus, as only low-multiplicity infections were examined (27). When disruption of arsenite-induced SG formation by D215N and ΔUL41 viruses was examined alongside WT virus at low multiplicity, the fraction of infected cells with SGs was ap-

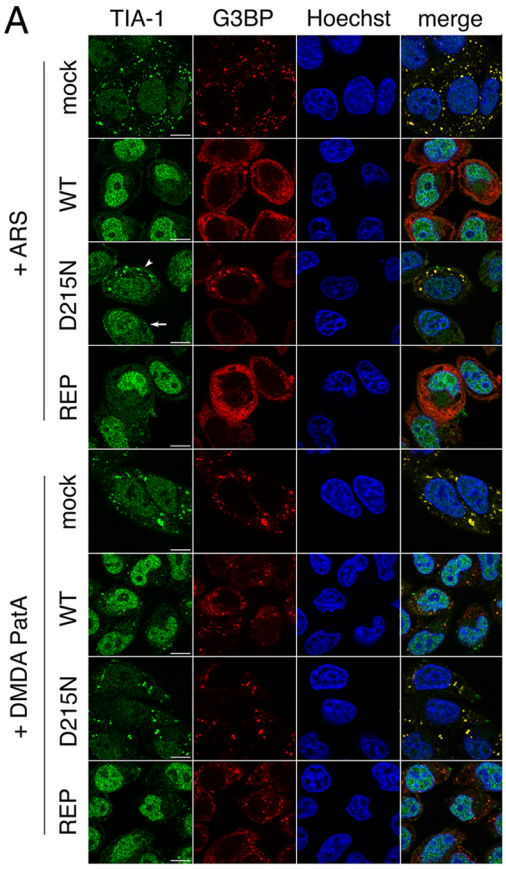

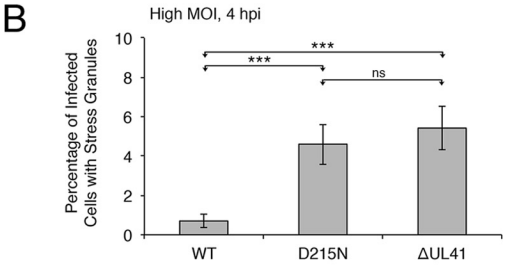

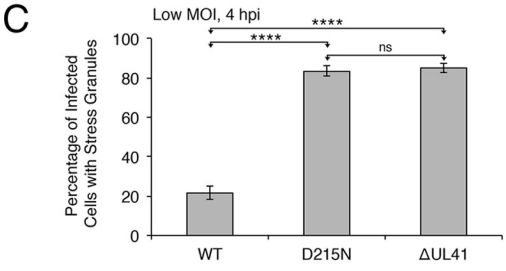

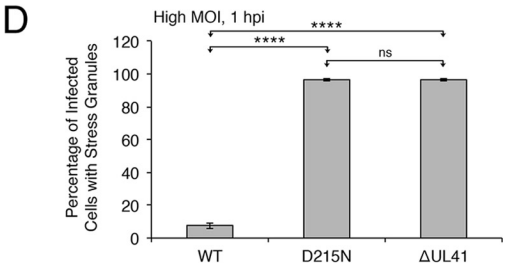

proximately 85% for both D215N and ΔUL41 viruses and was significantly greater than the fraction of infected cells with SGs observed for WT ($P < 0.0001$) (Fig. 3C). Finally, in high-multiplicity infections at 1 hpi, no disruption of arsenite-induced SG formation was detectable in either D215N or ΔUL41 virus infections (Fig. 3D). As both WT and D215NRep viruses outperformed D215N virus and D215N virus performed comparably to ΔUL41 virus in our analyses of disruption of arsenite-induced SG formation, we conclude that endoribonuclease activity is required in order for vhs to mediate this disruption. Disruption of arsenite-induced SG formation by both D215N and ΔUL41 virus depended on the multiplicity of infection used as well as the length of time that infections were allowed to proceed before arsenite treatment, raising the possibility that another viral component may contribute to this disruption.

In contrast to disruption of arsenite-induced SG formation, disruption of DMDA PatA-induced SG formation was not detected in cells infected at a high MOI with D215N virus (lower half of Fig. 3A). The SGs remaining in D215N infections treated with DMDA PatA contained both TIA-1 and G3BP, whereas those remaining in both WT and D215NRep virus infections were largely devoid of TIA-1, an SG modification we had previously observed in HSV-2-infected cells treated with PatA (26). Thus, in infected cells, vhs can disrupt SG formation caused by eIF2α phosphorylation-dependent translational arrest and modify SG formation caused by eIF2α phosphorylation-independent translational arrest, and vhs-mediated disruption/modification of SG formation in infected cells requires endoribonuclease activity.

Disassembly of preformed SGs can be mediated by vhs endoribonuclease activity. Conceivably, disruption of SG forma-

FIG 3 Analysis of SG formation in cells infected with vhs endoribonuclease-deficient HSV-2. (A) HeLa cells were mock inoculated or inoculated for 1 h with the indicated viruses at an MOI of 4. At 3.5 h after inoculation, infected cells were treated with either 500 mM arsenite (ARS) or 300 nM DMDA PatA. Thirty minutes later (4 hpi), infected cells were fixed and stained with goat polyclonal antiserum specific for TIA-1 and mouse monoclonal antibody specific for G3BP followed by staining with Alexa Fluor 488-conjugated donkey anti-goat IgG and Alexa Fluor 568-conjugated donkey anti-mouse IgG. Nuclei were stained with Hoechst 33342. Stained cells were examined by confocal microscopy, and with the exception of D215N virus infections treated with arsenite, representative images are shown. In the case of high-multiplicity D215N infections treated with arsenite, only approximately 8% of cells contained stress granules (arrowhead), while the majority of cells did not contain stress granules (arrow). Scale bars are 10 μm. (B) HeLa cells were inoculated for 1 h with the indicated viruses at an MOI of 4, treated with arsenite at 3.5 h after inoculation for 30 min, and then fixed (4 hpi) and stained as described for panel A. Samples were examined on an inverted epifluorescence microscope, and the percentage of cells with SGs was scored in 20 fields per sample. (C) HeLa cells were inoculated for 1 h with the indicated viruses at an MOI of 0.5, treated with arsenite at 3.5 h after inoculation for 30 min, and then fixed (4 hpi) and stained with goat polyclonal antiserum specific for TIA-1 and mouse monoclonal antibody specific for ICP27 followed by staining with Alexa Fluor 488-conjugated donkey anti-goat IgG and Alexa Fluor 568-conjugated donkey anti-mouse IgG. Nuclei were stained with Hoechst 33342. Samples were examined by confocal microscopy, and the percentage of infected cells (ICP27 positive) with SGs was scored in 30 fields per sample. (D) HeLa cells were inoculated for 1 h with the indicated viruses at an MOI of 4, treated with arsenite at 30 min after inoculation for 30 min, and then fixed (1 hpi) and stained as described for panel A. Samples were examined on an inverted epifluorescence microscope, and the percentage of cells with SGs was scored in 20 fields per sample. Error bars in panels B, C, and D indicate standard errors of the means. ****, $P < 0.0001$; ***, $P < 0.001$; ns, difference not statistically significant.

tion could arise as a result of either prevention of SG assembly, promotion of SG disassembly, or both of these activities. In our preceding analyses of SG formation during viral infection, cells were infected first and then SGs were induced, and so it was not possible to distinguish between these two possibilities. To specifically examine SG disassembly, we needed a method to generate stable SGs so that the ability of HSV-2 to disassemble these preformed SGs could be evaluated. SGs induced by PatA are known to be much more stable than SGs induced by phosphorylation of eIF2α, remaining for as long as 12 h in cultured cells in the absence of exogenous PatA (62). This stability likely results from incorporation of PatA into the resulting SGs via nonreversible binding to eIF4A (5).

To determine if HSV-2 infection could promote the disassembly of SGs, we pulse-treated HeLa cells with 300 nM DMDA PatA to induce SGs and then examined the fate of the resulting SGs following infection with HSV-2 or mock inoculum for 3 or 7 h (Fig. 4A). In DMDA PatA-treated, mock-infected controls, granules positive for both TIA-1 and G3BP were still detectable 7 h after removal of exogenous DMDA PatA (Fig. 4B) and showed no detectable differences in size in comparison to the granules in mock-infected controls at 3 h posttreatment (Fig. 4C). In contrast, the granules remaining in DMDA PatA-treated cells infected with WT HSV-2 for 3 h were smaller than those in their mock-infected counterparts and were further decreased in size at the later time point (Fig. 4B and C). Separate infectivity controls confirmed that all cells were infected in this experiment (data not shown). The decrease in SG size over time in infected cells indicates that HSV-2 is able to promote the disassembly of SGs. Furthermore, the granules remaining in DMDA PatA-treated cells infected for 7 h with HSV-2 were positive for G3BP but were largely devoid of TIA-1 (bottom row of images in Fig. 4B), suggesting that during HSV-2-mediated SG disassembly, TIA-1 departs in advance of G3BP.

To examine the requirement for HSV-2 vhs endoribonuclease activity in SG disassembly, a similar experiment was conducted comparing the sizes and compositions of DMDA PatA SGs following infection for 7 h with WT, D215N, or D215NRep virus. In these experiments, we used A549 cells that stably produce EGFP-G3BP1 (A549 SGG cells) (51) to enable us to simultaneously detect the SG markers G3BP and TIA-1 and the infectivity marker ICP27. A549 SGG cells also formed stable SGs in response to treatment with DMDA PatA (top two rows of images in Fig. 4D). Granules remaining in DMDA PatA-treated cells infected with WT or repair viruses were smaller than granules remaining in mock-infected cells (Fig. 4E) and were positive for G3BP but lacked TIA-1 (Fig. 4D). Granules remaining in DMDA PatA-treated cells infected with D215N were positive for both G3BP and TIA-1 and were similar in size to granules remaining in mock-infected cells (Fig. 4E). Taken together, these data indicate that (i) HSV-2 infection promotes the disassembly of preformed SGs, (ii) HSV-2-mediated SG disassembly requires vhs endoribonuclease activity, and (iii) during HSV-2-mediated SG disassembly, there is an order to the departure of SG components, with TIA-1 departing in advance of G3BP.

vhs localizes to SGs. If vhs is able to mediate the disassembly of preformed SGs, this predicts that vhs should localize to SGs. To examine the subcellular localization of vhs, we constructed a myc-tagged version of vhs carrying the D215N mutation (myc D215N vhs). Removal of vhs endoribonuclease activity was necessary in order to detect vhs and preserve SGs in transfected cells (data not shown). HeLa cells transfected with myc D215N vhs expression plasmids were treated with arsenite or DMDA PatA to induce SGs or left untreated and then fixed and stained for TIA-1 to detect SGs and the myc tag to detect vhs. Transfected cells in which the myc tag signal was clearly enriched at SGs over the myc tag signal in the surrounding cytoplasm were readily observed (Fig. 5A). This enrichment was not observed in nontransfected cells (Fig. 5B). In HeLa cells transfected with myc D215N vhs expression plasmid but not treated with arsenite or DMDA PatA, approximately 13% of transfected cells (25 of 195) formed SGs, presumably as a consequence of overexpression of myc D215N vhs. vhs also localized to these SGs (indicated by the asterisk in Fig. 5A). These data indicate that vhs can localize to SGs induced by either arsenite or DMDA PatA.

DISCUSSION

In this study, we demonstrate that endoribonuclease activity is specifically required in order for vhs to disrupt SG formation resulting from either eIF2α phosphorylation-dependent (arsenite) or eIF2α phosphorylation-independent (DMDA PatA) mechanisms of translational arrest in both transfected and infected cells. Disruption of DMDA PatA-induced SG formation by vhs in WT HSV-2 infected cells differed from that in vhs-transfected cells in that SG formation was not thoroughly disrupted. Instead, granules remained that contained G3BP but were largely devoid of TIA-1, as we had observed in our previous study (26). The increased level of vhs in transfected versus infected cells is a plausible explanation for the observed difference in disruption of DMDA PatA-induced SGs by vhs in transfected versus infected cells. If sufficient levels of vhs can thoroughly disrupt SG formation, then the granules remaining in HSV-2-infected cells that are subsequently treated with PatA or DMDA PatA represent intermediates in the assembly or, even more likely based on the results of our SG disassembly analyses, the disassembly of SGs.

In our previous studies, we observed that the number of cells containing SGs following transient overexpression of EGFP-TIA-1, a condition that leads to SG formation (10), was noticeably diminished when these cells were subsequently infected (26). Based on this result, we hypothesized that HSV-2 infection could promote the disassembly of preformed SGs. In support of this hypothesis, we demonstrate in this work that HSV-2 infection can promote SG disassembly in a manner that specifically requires vhs endoribonuclease activity. SG disassembly was evidenced by both a decrease in size of SGs over time as well as modification of SG composition. If vhs can promote SG disassembly, it follows that both vhs and XrnI should be able to localize to SGs. We demonstrate here that HSV-2 vhs does indeed have the ability to localize to SGs. While XrnI is often described as a marker of processing bodies, another type of cytoplasmic RNA granule often found associated with SGs (63), small amounts of XrnI have been found to localize to SGs (64).

Two noteworthy features of SG disassembly were discovered during the course of these studies. First, the requirement for vhs endoribonuclease activity in SG disassembly implies that removal of RNA from SGs promotes their disassembly and predicts that intact RNA is crucial for maintaining the integrity of these cytoplasmic compartments. It will be interesting to test whether other endoribonucleases promote SG disassembly and whether targeted delivery of an endoribonuclease to SGs can be developed as a means of disassembling SGs *in vivo*. Second, during SG disassem-

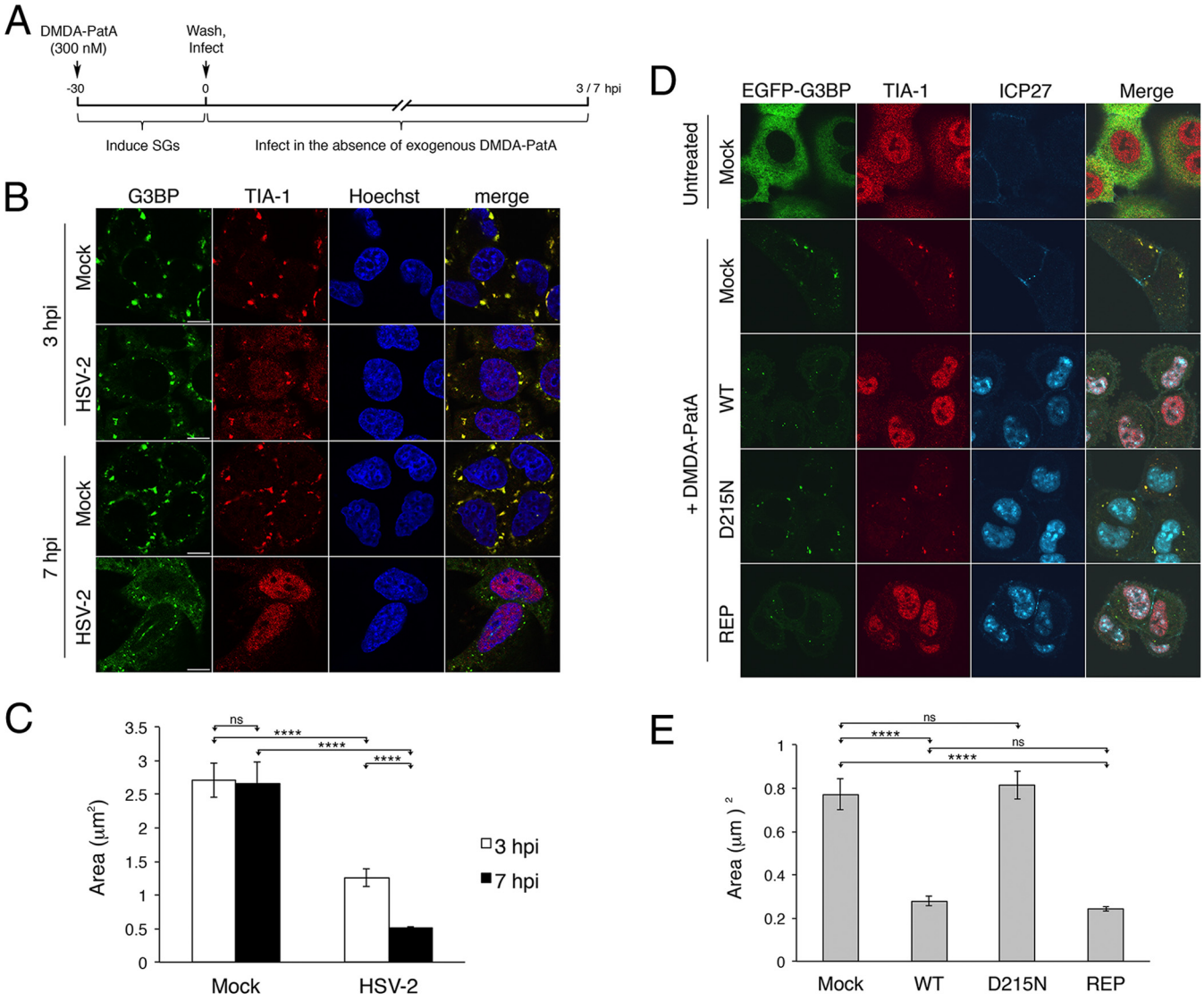

FIG 4 Disassembly of DMDA PatA SGs by HSV-2 requires vhs endoribonuclease activity. (A) Timeline of experiment. Note that the hours postinfection (hpi) shown refer to the total time in the presence of virus, including the 1-h inoculation period. (B) HeLa cells were pulse-treated with DMDA PatA to induce SGs and then infected at an MOI of 6 or mock infected in the absence of exogenous DMDA PatA. Cells were fixed at the indicated times after infection and stained with goat polyclonal antiserum specific for TIA-1 and mouse monoclonal antibody specific for G3BP followed by staining with Alexa Fluor 488-conjugated donkey anti-mouse IgG and Alexa Fluor 488-conjugated donkey anti-goat IgG. Nuclei were stained with Hoechst 33342. Stained cells were examined by confocal microscopy, and representative images are shown. Scale bars are 10 μm. (C) To compare the average sizes of the SGs following the conditions shown in panel B, the area of 100 SGs from each condition was measured using Fluoview 1.7.3.0 software and then averaged. Error bars indicate standard errors of the means. ****, $P < 0.0001$; ns, difference not statistically significant. (D) A549 SGG cells were pulse-treated with DMDA PatA to induce SGs. DMDA PatA-treated samples were then infected at an MOI of 4 with the indicated viruses or mock infected for 7 h in the absence of exogenous DMDA PatA. Untreated cells were mock infected for 7 h as well. Cells were fixed and stained with goat polyclonal antiserum specific for TIA-1 and mouse monoclonal antibody specific for ICP27 followed by staining with Alexa Fluor 488-conjugated donkey anti-goat IgG and Alexa Fluor 647-conjugated donkey anti-mouse IgG. Stained cells were examined by confocal microscopy, and representative images are shown. Scale bars are 10 μm. (E) To compare the average sizes of the SGs following the conditions shown in panel D, the area of 100 SGs from each condition was measured using Fluoview 1.7.3.0 software and then averaged. Error bars indicate standard errors of the means. ****, $P < 0.0001$; ns, difference not statistically significant.

bly there is an ordered departure of SG components, with TIA-1 departing before G3BP. Determination of whether this departure order applies to disassembly of eIF2α phosphorylation-induced SGs as well as whether a departure order can also be applied to other SG components, including RNA, will be crucial in order to establish that ordered departure of components is a general feature of SG disassembly. Very recently, the structure of arsenite-induced SGs was examined by superresolution microscopy, revealing that these SGs have a stable core structure, enriched in G3BP, surrounded by a more dynamic shell (24). If SGs induced by PatA/DMDA PatA share this structure, then the G3BP-containing granules remaining after vhs-mediated disassembly may represent the SG cores defined by this pioneering study. Isolated SG cores were demonstrated to contain poly(A)$^+$ RNA but were found to be largely resistant to treatment with a cocktail of RNase A and RNase T_1 *in vitro*, suggesting that protein-protein interac-

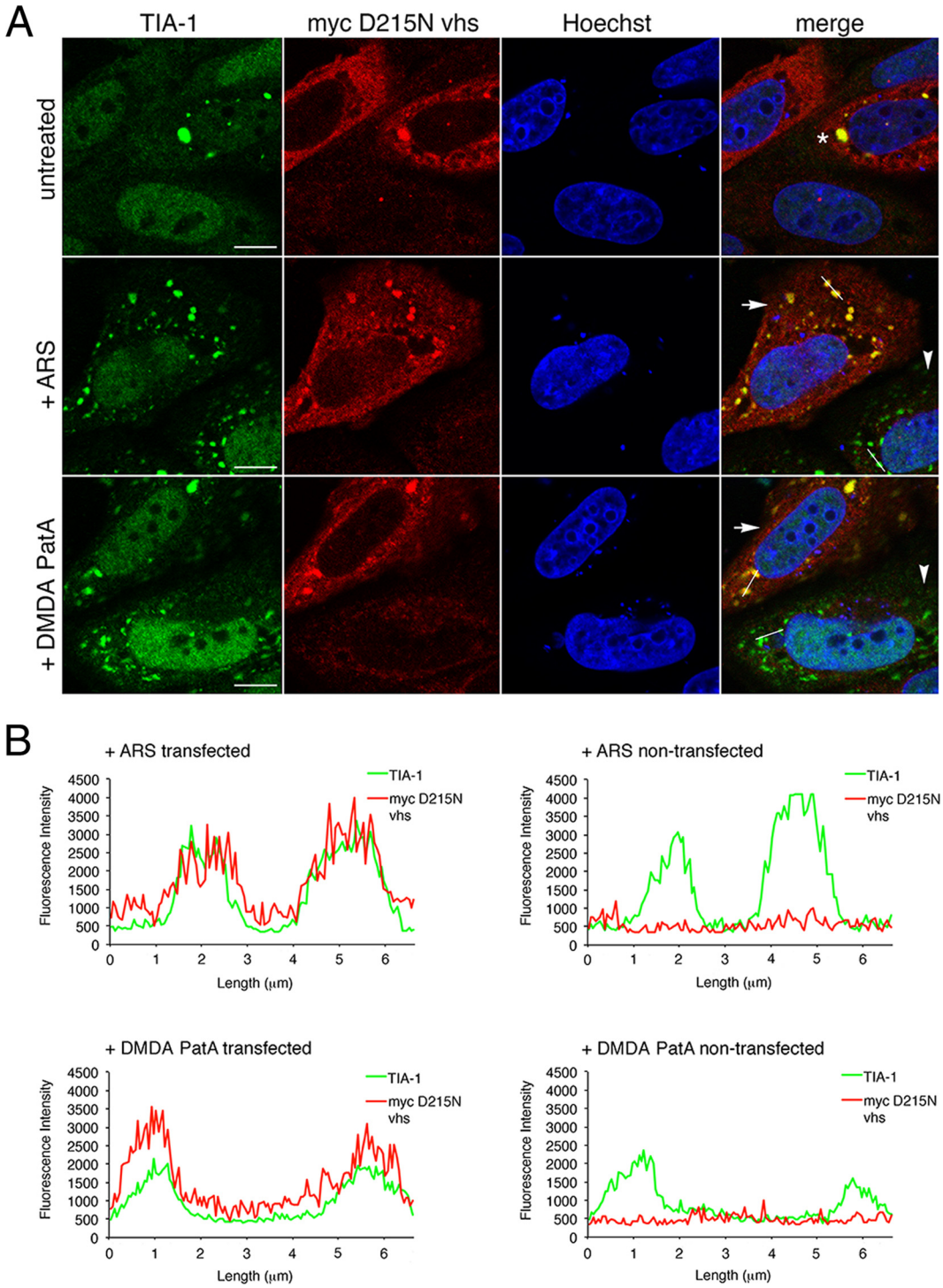

FIG 5 vhs localizes to SGs. (A) HeLa cells were transfected with a myc-tagged D215N vhs expression construct. At 40 h posttransfection, cells were treated with 0.5 mM arsenite (ARS) or 300 nM DMDA PatA for 30 min or left untreated and then fixed and stained with goat polyclonal antiserum specific for TIA-1 and mouse monoclonal antibody specific for the myc tag followed by staining with Alexa Fluor 488-conjugated donkey anti-goat IgG and Alexa Fluor 568-conjugated donkey anti-mouse IgG. Nuclei were stained with Hoechst 33342. Stained cells were examined by confocal microscopy. Arrows indicate transfected cells, arrowheads indicate nontransfected cells, and an asterisk indicates an SG arising from overexpression of myc D215N vhs, detectable in approximately 13% of untreated, transfected cells. Scale bars are 10 μm. (B) The fluorescence intensity was measured across an approximately 6.5-μm line drawn between adjacent SGs in transfected or nontransfected cells using Fluoview 1.7.3.0 software. The locations of the measurement lines are shown on the merged image panels.

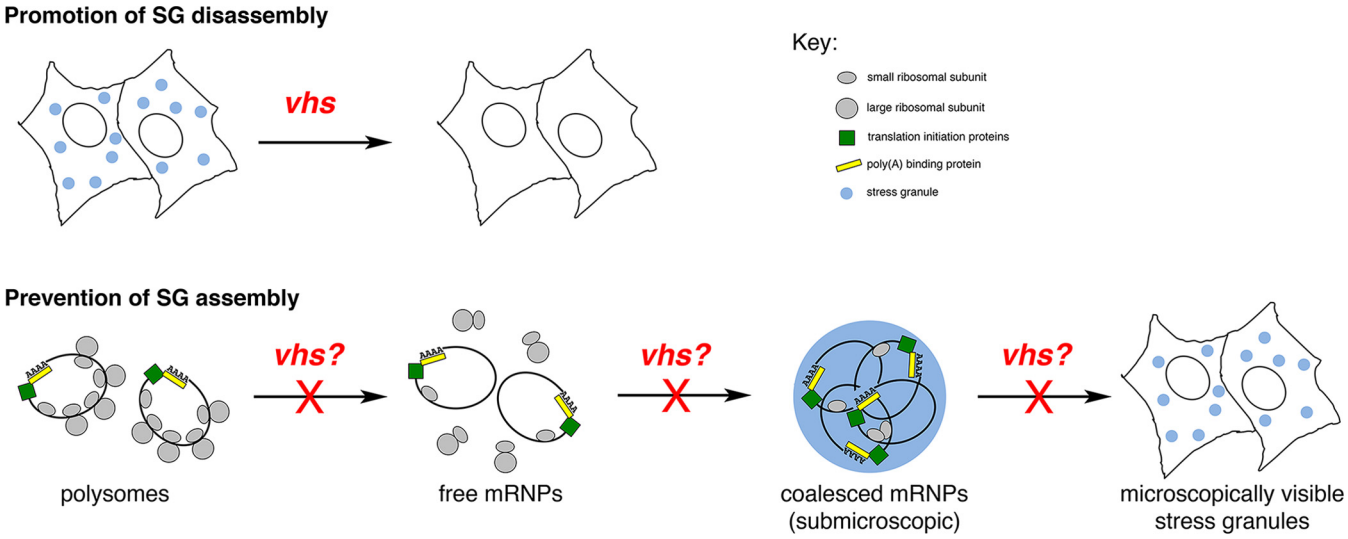

FIG 6 Model of vhs endoribonuclease-mediated disruption of SG formation. Two different modes of disruption ascribable to vhs are depicted: promotion of SG disassembly (top) and prevention of SG assembly (bottom). vhs endoribonuclease activity in concert with XrnI exonuclease activity promotes the destruction of mRNAs present in existing SGs, which leads to their disassembly. This mode of vhs-mediated disruption of SG formation has been verified by work reported in this article. An additional possibility that remains to be experimentally verified is that vhs/XrnI activities promote the destruction of mRNAs present in polysomes, free mRNPs, or submicroscopic coalesced mRNPs, which prevents the ensuing step in the SG assembly pathway. For simplicity, microscopically visible SGs as well as submicroscopic SG nucleation sites are both represented as blue circles; visible SGs are often irregular in shape and are variable in size.

tions could maintain the integrity of SG cores. Thus, it is plausible that SG cores could remain after destruction of their RNA by vhs. It will be of considerable interest to establish whether RNA is present in the G3BP-containing granules remaining after vhs-mediated disassembly.

Our model for the two modes in which the endoribonuclease activity of vhs may be operating to disrupt SG formation is presented in Fig. 6. The top mode, promotion of SG disassembly, has been experimentally verified by our studies. The bottom mode, prevention of SG assembly, can conceivably be operating in addition to promotion of SG disassembly. This model is in keeping with the crucial roles played by RNA in initiating SG formation and, as we propose in this work, in maintaining SG structure.

While the model presented in Fig. 6 focuses on the contribution of vhs to the disruption of SG formation, it is conceivable that another viral component(s) also contributes to this disruption. The data presented in Fig. 3 support the existence of such a component. We have observed that disruption of SG formation continues to late times postinfection (26), when the endoribonuclease activity of vhs is predicted to be suppressed via the interaction of vhs with VP16 and VP22 (65–68). Thus, another viral component may be required later in infection to ensure the continued disruption of SG formation. The identity of this contributor remains to be determined; however, candidate viral proteins include those that localize to SGs (ICP27 and Us3) (27) as well as those involved in counteracting eIF2 kinases and the resulting phosphorylation of eIF2α (Us11, gB, and ICP34.5) (69–72). In this regard, it is noteworthy that influenza A virus deploys multiple proteins to disrupt SG formation throughout viral replication (62, 73).

HSV strains carrying large deletions in the UL41 gene encoding vhs have been reported to have two particular attributes: cells infected with these viruses form spontaneous SGs late in infection (27, 41, 74), and virus is unable to block activation of double-stranded RNA-dependent eIF2 kinase (protein kinase R [PKR]) that arises as a result of infection (68, 75). In keeping with the first attribute, we demonstrate here that specific removal of vhs endoribonuclease activity also results in spontaneous SG formation. Roizman and colleagues have proposed that vhs, via its endoribonuclease activity, can clear self-annealing RNAs that carry double-stranded stretches capable of activating PKR (68). Furthermore, Smiley and colleagues have recently demonstrated that PKR is essential for the formation of spontaneous SGs in cells infected with an HSV-1 vhs mutant (75), suggesting that these two attributes are interrelated, with the first being a consequence of the second. However, it is important to bear in mind that SGs are being increasingly viewed as more than a mere consequence of a cell's stress response or a temporary storage depot for mRNPs. Two independent research groups have shown that SGs can promote innate immune responses (76–79). This has led to the proposal that SGs serve as platforms for recognizing and responding to viral infections (80), which may explain why so many viruses destroy or modify SGs during infection and necessitates a better understanding of SG biology.

ACKNOWLEDGMENTS

This work was supported by Canadian Institutes of Health Research operating grant 93804, Natural Sciences and Engineering Council of Canada Discovery grant 418719, and Canada Foundation for Innovation award 16389.

We thank D. W. Wilson, Albert Einstein College of Medicine, for vhs antisera, N. Osterreidder, Freie Universität Berlin, for plasmid pEP-Kan-S2, and C. McCormick, Dalhousie University, for A549 cells stably producing EGFP-G3BP1.

FUNDING INFORMATION

This work, including the efforts of Bruce W. Banfield, was funded by Natural Sciences and Engineering Research Council of Canada (NSERC) (418719). This work, including the efforts of Bruce W. Banfield, was funded by Canadian Institutes of Health Research (CIHR) (93804). This work, including the efforts of Bruce W. Banfield, was funded by Canada Foundation for Innovation (CFI) (16389).

REFERENCES

1. **Anderson P, Kedersha N.** 2008. Stress granules: the Tao of RNA triage. Trends Biochem Sci **33:**141–150. http://dx.doi.org/10.1016/j.tibs.2007.12.003.
2. **Wek RC, Jiang HY, Anthony TG.** 2006. Coping with stress: eIF2 kinases and translational control. Biochem Soc Trans **34:**7–11. http://dx.doi.org/10.1042/BST0340007.
3. **Kedersha N, Ivanov P, Anderson P.** 2013. Stress granules and cell signaling: more than just a passing phase? Trends Biochem Sci **38:**494–506. http://dx.doi.org/10.1016/j.tibs.2013.07.004.
4. **Mazroui R, Sukarieh R, Bordeleau ME, Kaufman RJ, Northcote P, Tanaka J, Gallouzi I, Pelletier J.** 2006. Inhibition of ribosome recruitment induces stress granule formation independently of eukaryotic initiation factor 2alpha phosphorylation. Mol Biol Cell **17:**4212–4219. http://dx.doi.org/10.1091/mbc.E06-04-0318.
5. **Dang Y, Kedersha N, Low WK, Romo D, Gorospe M, Kaufman R, Anderson P, Liu JO.** 2006. Eukaryotic initiation factor 2alpha-independent pathway of stress granule induction by the natural product pateamine A. J Biol Chem **281:**32870–32878. http://dx.doi.org/10.1074/jbc.M606149200.
6. **Kedersha N, Cho MR, Li W, Yacono PW, Chen S, Gilks N, Golan DE, Anderson P.** 2000. Dynamic shuttling of TIA-1 accompanies the recruitment of mRNA to mammalian stress granules. J Cell Biol **151:**1257–1268. http://dx.doi.org/10.1083/jcb.151.6.1257.
7. **Bounedjah O, Desforges B, Wu TD, Pioche-Durieu C, Marco S, Hamon L, Curmi PA, Guerquin-Kern JL, Pietrement O, Pastre D.** 2014. Free mRNA in excess upon polysome dissociation is a scaffold for protein multimerization to form stress granules. Nucleic Acids Res **42:**8678–8691. http://dx.doi.org/10.1093/nar/gku582.
8. **Schwartz JC, Wang X, Podell ER, Cech TR.** 2013. RNA seeds higher-order assembly of FUS protein. Cell Rep **5:**918–925. http://dx.doi.org/10.1016/j.celrep.2013.11.017.
9. **Tourriere H, Chebli K, Zekri L, Courselaud B, Blanchard JM, Bertrand E, Tazi J.** 2003. The RasGAP-associated endoribonuclease G3BP assembles stress granules. J Cell Biol **160:**823–831. http://dx.doi.org/10.1083/jcb.200212128.
10. **Gilks N, Kedersha N, Ayodele M, Shen L, Stoecklin G, Dember LM, Anderson P.** 2004. Stress granule assembly is mediated by prion-like aggregation of TIA-1. Mol Biol Cell **15:**5383–5398. http://dx.doi.org/10.1091/mbc.E04-08-0715.
11. **De Leeuw F, Zhang T, Wauquier C, Huez G, Kruys V, Gueydan C.** 2007. The cold-inducible RNA-binding protein migrates from the nucleus to cytoplasmic stress granules by a methylation-dependent mechanism and acts as a translational repressor. Exp Cell Res **313:**4130–4144. http://dx.doi.org/10.1016/j.yexcr.2007.09.017.
12. **Dolzhanskaya N, Merz G, Aletta JM, Denman RB.** 2006. Methylation regulates the intracellular protein-protein and protein-RNA interactions of FMRP. J Cell Sci **119:**1933–1946. http://dx.doi.org/10.1242/jcs.02882.
13. **Kwon S, Zhang Y, Matthias P.** 2007. The deacetylase HDAC6 is a novel critical component of stress granules involved in the stress response. Genes Dev **21:**3381–3394. http://dx.doi.org/10.1101/gad.461107.
14. **Ohn T, Kedersha N, Hickman T, Tisdale S, Anderson P.** 2008. A functional RNAi screen links O-GlcNAc modification of ribosomal proteins to stress granule and processing body assembly. Nat Cell Biol **10:**1224–1231. http://dx.doi.org/10.1038/ncb1783.
15. **Isabelle M, Gagne JP, Gallouzi IE, Poirier GG.** 2012. Quantitative proteomics and dynamic imaging reveal that G3BP-mediated stress granule assembly is poly(ADP-ribose)-dependent following exposure to MNNG-induced DNA alkylation. J Cell Sci **125:**4555–4566. http://dx.doi.org/10.1242/jcs.106963.
16. **Leung A, Todorova T, Ando Y, Chang P.** 2012. Poly(ADP-ribose) regulates post-transcriptional gene regulation in the cytoplasm. RNA Biol **9:**542–548. http://dx.doi.org/10.4161/rna.19899.
17. **Leung AK, Vyas S, Rood JE, Bhutkar A, Sharp PA, Chang P.** 2011. Poly(ADP-ribose) regulates stress responses and microRNA activity in the cytoplasm. Mol Cell **42:**489–499. http://dx.doi.org/10.1016/j.molcel.2011.04.015.
18. **Kroschwald S, Maharana S, Mateju D, Malinovska L, Nuske E, Poser I, Richter D, Alberti S.** 2015. Promiscuous interactions and protein disaggregases determine the material state of stress-inducible RNP granules. eLife **4:**e06807. http://dx.doi.org/10.7554/eLife.06807.
19. **Ivanov PA, Chudinova EM, Nadezhdina ES.** 2003. Disruption of microtubules inhibits cytoplasmic ribonucleoprotein stress granule formation. Exp Cell Res **290:**227–233. http://dx.doi.org/10.1016/S0014-4827(03)00290-8.
20. **Ivanov PA, Chudinova EM, Nadezhdina ES.** 2003. RNP stress-granule formation is inhibited by microtubule disruption. Cell Biol Int **27:**207–208. http://dx.doi.org/10.1016/S1065-6995(02)00341-4.
21. **Chernov KG, Barbet A, Hamon L, Ovchinnikov LP, Curmi PA, Pastre D.** 2009. Role of microtubules in stress granule assembly: microtubule dynamical instability favors the formation of micrometric stress granules in cells. J Biol Chem **284:**36569–36580. http://dx.doi.org/10.1074/jbc.M109.042879.
22. **Loschi M, Leishman CC, Berardone N, Boccaccio GL.** 2009. Dynein and kinesin regulate stress-granule and P-body dynamics. J Cell Sci **122:**3973–3982. http://dx.doi.org/10.1242/jcs.051383.
23. **Rajgor D, Shanahan CM.** 2014. RNA granules and cytoskeletal links. Biochem Soc Trans **42:**1206–1210. http://dx.doi.org/10.1042/BST20140067.
24. **Jain S, Wheeler JR, Walters RW, Agrawal A, Barsic A, Parker R.** 2016. ATPase-modulated stress granules contain a diverse proteome and substructure. Cell **164:**487–498. http://dx.doi.org/10.1016/j.cell.2015.12.038.
25. **Wippich F, Bodenmiller B, Trajkovska MG, Wanka S, Aebersold R, Pelkmans L.** 2013. Dual specificity kinase DYRK3 couples stress granule condensation/dissolution to mTORC1 signaling. Cell **152:**791–805. http://dx.doi.org/10.1016/j.cell.2013.01.033.
26. **Finnen RL, Pangka KR, Banfield BW.** 2012. Herpes simplex virus 2 infection impacts stress granule accumulation. J Virol **86:**8119–8130. http://dx.doi.org/10.1128/JVI.00313-12.
27. **Finnen RL, Hay TJ, Dauber B, Smiley JR, Banfield BW.** 2014. The herpes simplex virus 2 virion-associated ribonuclease vhs interferes with stress granule formation. J Virol **88:**12727–12739. http://dx.doi.org/10.1128/JVI.01554-14.
28. **Everly DN, Jr, Feng P, Mian IS, Read GS.** 2002. mRNA degradation by the virion host shutoff (Vhs) protein of herpes simplex virus: genetic and biochemical evidence that Vhs is a nuclease. J Virol **76:**8560–8571. http://dx.doi.org/10.1128/JVI.76.17.8560-8571.2002.
29. **Zelus BD, Stewart RS, Ross J.** 1996. The virion host shutoff protein of herpes simplex virus type 1: messenger ribonucleolytic activity in vitro. J Virol **70:**2411–2419.
30. **McGeoch DJ, Dalrymple MA, Davison AJ, Dolan A, Frame MC, McNab D, Perry LJ, Scott JE, Taylor P.** 1988. The complete DNA sequence of the long unique region in the genome of herpes simplex virus type 1. J Gen Virol **69:**1531–1574. http://dx.doi.org/10.1099/0022-1317-69-7-1531.
31. **Morse LS, Pereira L, Roizman B, Schaffer PA.** 1978. Anatomy of herpes simplex virus (HSV) DNA. X. Mapping of viral genes by analysis of polypeptides and functions specified by HSV-1 × HSV-2 recombinants. J Virol **26:**389–410.
32. **Read GS, Patterson M.** 2007. Packaging of the virion host shutoff (Vhs) protein of herpes simplex virus: two forms of the Vhs polypeptide are associated with intranuclear B and C capsids, but only one is associated with enveloped virions. J Virol **81:**1148–1161. http://dx.doi.org/10.1128/JVI.01812-06.
33. **Smibert CA, Johnson DC, Smiley JR.** 1992. Identification and characterization of the virion-induced host shutoff product of herpes simplex virus gene UL41. J Gen Virol **73:**467–470. http://dx.doi.org/10.1099/0022-1317-73-2-467.
34. **Abernathy E, Glaunsinger B.** 2015. Emerging roles for RNA degradation in viral replication and antiviral defense. Virology **479–480:**600–608. http://dx.doi.org/10.1016/j.virol.2015.02.007.
35. **Gaglia MM, Covarrubias S, Wong W, Glaunsinger BA.** 2012. A common strategy for host RNA degradation by divergent viruses. J Virol **86:**9527–9530. http://dx.doi.org/10.1128/JVI.01230-12.
36. **Spencer CA, Dahmus ME, Rice SA.** 1997. Repression of host RNA polymerase II transcription by herpes simplex virus type 1. J Virol **71:**2031–2040.
37. **Hardy WR, Sandri-Goldin RM.** 1994. Herpes simplex virus inhibits host cell splicing, and regulatory protein ICP27 is required for this effect. J Virol **68:**7790–7799.

38. **Doepker RC, Hsu WL, Saffran HA, Smiley JR.** 2004. Herpes simplex virus virion host shutoff protein is stimulated by translation initiation factors eIF4B and eIF4H. J Virol **78:**4684–4699. http://dx.doi.org/10.1128/JVI.78.9.4684-4699.2004.
39. **Feng P, Everly DN, Jr, Read GS.** 2005. mRNA decay during herpes simplex virus (HSV) infections: protein-protein interactions involving the HSV virion host shutoff protein and translation factors eIF4H and eIF4A. J Virol **79:**9651–9664. http://dx.doi.org/10.1128/JVI.79.15.9651-9664.2005.
40. **Page HG, Read GS.** 2010. The virion host shutoff endonuclease (UL41) of herpes simplex virus interacts with the cellular cap-binding complex eIF4F. J Virol **84:**6886–6890. http://dx.doi.org/10.1128/JVI.00166-10.
41. **Dauber B, Pelletier J, Smiley JR.** 2011. The herpes simplex virus 1 vhs protein enhances translation of viral true late mRNAs and virus production in a cell type-dependent manner. J Virol **85:**5363–5373. http://dx.doi.org/10.1128/JVI.00115-11.
42. **Dauber B, Saffran HA, Smiley JR.** 2014. The herpes simplex virus 1 virion host shutoff protein enhances translation of viral late mRNAs by preventing mRNA overload. J Virol **88:**9624–9632. http://dx.doi.org/10.1128/JVI.01350-14.
43. **Saffran HA, Read GS, Smiley JR.** 2010. Evidence for translational regulation by the herpes simplex virus virion host shutoff protein. J Virol **84:**6041–6049. http://dx.doi.org/10.1128/JVI.01819-09.
44. **Elgadi MM, Smiley JR.** 1999. Picornavirus internal ribosome entry site elements target RNA cleavage events induced by the herpes simplex virus virion host shutoff protein. J Virol **73:**9222–9231.
45. **Kedersha N, Anderson P.** 2009. Regulation of translation by stress granules and processing bodies. Prog Mol Biol Transl Sci **90:**155–185. http://dx.doi.org/10.1016/S1877-1173(09)90004-7.
46. **Everly DN, Jr, Read GS.** 1999. Site-directed mutagenesis of the virion host shutoff gene (UL41) of herpes simplex virus (HSV): analysis of functional differences between HSV type 1 (HSV-1) and HSV-2 alleles. J Virol **73:**9117–9129.
47. **Hosfield DJ, Mol CD, Shen B, Tainer JA.** 1998. Structure of the DNA repair and replication endonuclease and exonuclease FEN-1: coupling DNA and PCNA binding to FEN-1 activity. Cell **95:**135–146. http://dx.doi.org/10.1016/S0092-8674(00)81789-4.
48. **Tsutakawa SE, Classen S, Chapados BR, Arvai AS, Finger LD, Guenther G, Tomlinson CG, Thompson P, Sarker AH, Shen B, Cooper PK, Grasby JA, Tainer JA.** 2011. Human flap endonuclease structures, DNA double-base flipping, and a unified understanding of the FEN1 superfamily. Cell **145:**198–211. http://dx.doi.org/10.1016/j.cell.2011.03.004.
49. **Everett RD, Fenwick ML.** 1990. Comparative DNA sequence analysis of the host shutoff genes of different strains of herpes simplex virus: type 2 strain HG52 encodes a truncated UL41 product. J Gen Virol **71:**1387–1390. http://dx.doi.org/10.1099/0022-1317-71-6-1387.
50. **Korom M, Wylie KM, Morrison LA.** 2008. Selective ablation of virion host shutoff protein RNase activity attenuates herpes simplex virus 2 in mice. J Virol **82:**3642–3653. http://dx.doi.org/10.1128/JVI.02409-07.
51. **Khaperskyy DA, Hatchette TF, McCormick C.** 2012. Influenza A virus inhibits cytoplasmic stress granule formation. FASEB J **26:**1629–1639. http://dx.doi.org/10.1096/fj.11-196915.
52. **Le Sage V, Jung M, Alter JD, Wills EG, Johnston SM, Kawaguchi Y, Baines JD, Banfield BW.** 2013. The herpes simplex virus 2 UL21 protein is essential for virus propagation. J Virol **87:**5904–5915. http://dx.doi.org/10.1128/JVI.03489-12.
53. **Tischer BK, Smith GA, Osterrieder N.** 2010. En passant mutagenesis: a two step markerless Red recombination system. Methods Mol Biol **634:**421–430. http://dx.doi.org/10.1007/978-1-60761-652-8_30.
54. **Romo D, Choi NS, Li S, Buchler I, Shi Z, Liu JO.** 2004. Evidence for separate binding and scaffolding domains in the immunosuppressive and antitumor marine natural product, pateamine A: design, synthesis, and activity studies leading to a potent simplified derivative. J Am Chem Soc **126:**10582–10588. http://dx.doi.org/10.1021/ja040065s.
55. **Finnen RL, Roy BB, Zhang H, Banfield BW.** 2010. Analysis of filamentous process induction and nuclear localization properties of the HSV-2 serine/threonine kinase Us3. Virology **397:**23–33. http://dx.doi.org/10.1016/j.virol.2009.11.012.
56. **Lee GE, Church GA, Wilson DW.** 2003. A subpopulation of tegument protein vhs localizes to detergent-insoluble lipid rafts in herpes simplex virus-infected cells. J Virol **77:**2038–2045. http://dx.doi.org/10.1128/JVI.77.3.2038-2045.2003.
57. **Lyman MG, Demmin GL, Banfield BW.** 2003. The attenuated pseudorabies virus strain Bartha fails to package the tegument proteins Us3 and VP22. J Virol **77:**1403–1414. http://dx.doi.org/10.1128/JVI.77.2.1403-1414.2003.
58. **McEwen E, Kedersha N, Song B, Scheuner D, Gilks N, Han A, Chen JJ, Anderson P, Kaufman RJ.** 2005. Heme-regulated inhibitor kinase-mediated phosphorylation of eukaryotic translation initiation factor 2 inhibits translation, induces stress granule formation, and mediates survival upon arsenite exposure. J Biol Chem **280:**16925–16933. http://dx.doi.org/10.1074/jbc.M412882200.
59. **Bordeleau ME, Cencic R, Lindqvist L, Oberer M, Northcote P, Wagner G, Pelletier J.** 2006. RNA-mediated sequestration of the RNA helicase eIF4A by pateamine A inhibits translation initiation. Chem Biol **13:**1287–1295. http://dx.doi.org/10.1016/j.chembiol.2006.10.005.
60. **Bordeleau ME, Matthews J, Wojnar JM, Lindqvist L, Novac O, Jankowsky E, Sonenberg N, Northcote P, Teesdale-Spittle P, Pelletier J.** 2005. Stimulation of mammalian translation initiation factor eIF4A activity by a small molecule inhibitor of eukaryotic translation. Proc Natl Acad Sci U S A **102:**10460–10465. http://dx.doi.org/10.1073/pnas.0504249102.
61. **Low WK, Dang Y, Schneider-Poetsch T, Shi Z, Choi NS, Merrick WC, Romo D, Liu JO.** 2005. Inhibition of eukaryotic translation initiation by the marine natural product pateamine A. Mol Cell **20:**709–722. http://dx.doi.org/10.1016/j.molcel.2005.10.008.
62. **Khaperskyy DA, Emara MM, Johnston BP, Anderson P, Hatchette TF, McCormick C.** 2014. Influenza a virus host shutoff disables antiviral stress-induced translation arrest. PLoS Pathog **10:**e1004217. http://dx.doi.org/10.1371/journal.ppat.1004217.
63. **Stoecklin G, Kedersha N.** 2013. Relationship of GW/P-bodies with stress granules. Adv Exp Med Biol **768:**197–211. http://dx.doi.org/10.1007/978-1-4614-5107-5_12.
64. **Kedersha N, Stoecklin G, Ayodele M, Yacono P, Lykke-Andersen J, Fritzler MJ, Scheuner D, Kaufman RJ, Golan DE, Anderson P.** 2005. Stress granules and processing bodies are dynamically linked sites of mRNP remodeling. J Cell Biol **169:**871–884. http://dx.doi.org/10.1083/jcb.200502088.
65. **Knez J, Bilan PT, Capone JP.** 2003. A single amino acid substitution in herpes simplex virus type 1 VP16 inhibits binding to the virion host shutoff protein and is incompatible with virus growth. J Virol **77:**2892–2902. http://dx.doi.org/10.1128/JVI.77.5.2892-2902.2003.
66. **Lam Q, Smibert CA, Koop KE, Lavery C, Capone JP, Weinheimer SP, Smiley JR.** 1996. Herpes simplex virus VP16 rescues viral mRNA from destruction by the virion host shutoff function. EMBO J **15:**2575–2581.
67. **Smibert CA, Popova B, Xiao P, Capone JP, Smiley JR.** 1994. Herpes simplex virus VP16 forms a complex with the virion host shutoff protein vhs. J Virol **68:**2339–2346.
68. **Sciortino MT, Taddeo B, Giuffre-Cuculletto M, Medici MA, Mastino A, Roizman B.** 2007. Replication-competent herpes simplex virus 1 isolates selected from cells transfected with a bacterial artificial chromosome DNA lacking only the UL49 gene vary with respect to the defect in the UL41 gene encoding host shutoff RNase. J Virol **81:**10924–10932. http://dx.doi.org/10.1128/JVI.01239-07.
69. **Cassady KA, Gross M.** 2002. The herpes simplex virus type 1 U(S)11 protein interacts with protein kinase R in infected cells and requires a 30-amino-acid sequence adjacent to a kinase substrate domain. J Virol **76:**2029–2035. http://dx.doi.org/10.1128/jvi.76.5.2029-2035.2002.
70. **Cassady KA, Gross M, Roizman B.** 1998. The herpes simplex virus US11 protein effectively compensates for the gamma1(34.5) gene if present before activation of protein kinase R by precluding its phosphorylation and that of the alpha subunit of eukaryotic translation initiation factor 2. J Virol **72:**8620–8626.
71. **Mulvey M, Arias C, Mohr I.** 2007. Maintenance of endoplasmic reticulum (ER) homeostasis in herpes simplex virus type 1-infected cells through the association of a viral glycoprotein with PERK, a cellular ER stress sensor. J Virol **81:**3377–3390. http://dx.doi.org/10.1128/JVI.02191-06.
72. **He B, Gross M, Roizman B.** 1997. The gamma(1)34.5 protein of herpes simplex virus 1 complexes with protein phosphatase 1alpha to dephosphorylate the alpha subunit of the eukaryotic translation initiation factor 2 and preclude the shutoff of protein synthesis by double-stranded RNA-activated protein kinase. Proc Natl Acad Sci U S A **94:**843–848. http://dx.doi.org/10.1073/pnas.94.3.843.
73. **Khaperskyy DA, McCormick C.** 2015. Timing is everything: coordinated control of host shutoff by influenza A virus NS1 and PA-X proteins. J Virol **89:**6528–6531. http://dx.doi.org/10.1128/JVI.00386-15.

74. **Esclatine A, Taddeo B, Roizman B.** 2004. Herpes simplex virus 1 induces cytoplasmic accumulation of TIA-1/TIAR and both synthesis and cytoplasmic accumulation of tristetraprolin, two cellular proteins that bind and destabilize AU-rich RNAs. J Virol **78:**8582–8592. http://dx.doi.org/10.1128/JVI.78.16.8582-8592.2004.
75. **Dauber B, Poon D, Dos Santos T, Duguay BA, Mehta N, Saffran HA, Smiley JR.** 2016. The herpes simplex virus virion host shutoff protein enhances translation of viral true late mRNAs independently of suppressing protein kinase R and stress granule formation. J Virol **90:**6049–6057. http://dx.doi.org/10.1128/JVI.03180-15.
76. **Onomoto K, Jogi M, Yoo JS, Narita R, Morimoto S, Takemura A, Sambhara S, Kawaguchi A, Osari S, Nagata K, Matsumiya T, Namiki H, Yoneyama M, Fujita T.** 2012. Critical role of an antiviral stress granule containing RIG-I and PKR in viral detection and innate immunity. PLoS One **7:**e43031. http://dx.doi.org/10.1371/journal.pone.0043031.
77. **Oh SW, Onomoto K, Wakimoto M, Onoguchi K, Ishidate F, Fujiwara T, Yoneyama M, Kato H, Fujita T.** 2016. Leader-containing uncapped viral transcript activates RIG-I in antiviral stress granules. PLoS Pathog **12:**e1005444. http://dx.doi.org/10.1371/journal.ppat.1005444.
78. **Reineke LC, Kedersha N, Langereis MA, van Kuppeveld FJ, Lloyd RE.** 2015. Stress granules regulate double-stranded RNA-dependent protein kinase activation through a complex containing G3BP1 and Caprin1. mBio **6:**e02486. http://dx.doi.org/10.1128/mBio.02486-14.
79. **Reineke LC, Lloyd RE.** 2015. The stress granule protein G3BP1 recruits protein kinase R to promote multiple innate immune antiviral responses. J Virol **89:**2575–2589. http://dx.doi.org/10.1128/JVI.02791-14.
80. **Onomoto K, Yoneyama M, Fung G, Kato H, Fujita T.** 2014. Antiviral innate immunity and stress granule responses. Trends Immunol **35:**420–428. http://dx.doi.org/10.1016/j.it.2014.07.006.